Journal of Statistical Physics, Vol. 74, Nos. 3/4, 1994

Brownian Dynamics Simulations of Colloidal Hard Spheres. Effects of Sample Dimensionality on Self-Diffusion

W. Schaertl[1] and H. Sillescu[1]

Received April 27, 1993; final September 21, 1993

The self-diffusion coefficients of colloidal hard spheres were determined by Brownian dynamics (BD) computer simulations using a new efficient algorithm for treatment of the hard-sphere interactions. Calculations were done on an Apple PC type MacIIcx and on a MicroVAX 3000, considering samples in two and three dimensions at varying particle concentrations. Our results in three dimensions are compared with experimental results from our own group which were obtained by forced Rayleigh scattering (FRS), and with numerical results from a dynamical Monte Carlo simulation by Cichocki and Hinsen. Good agreement with the latter was found for particle volume fractions up to 0.40. Differences in the dynamical behavior of our numerically treated 2D and 3D samples are discussed using a simple geometrical model to enable comparison of particle concentrations in samples with different dimensionality.

KEY WORDS: BD simulations; colloidal hard spheres; dimensionality.

1. INTRODUCTION

Colloidal spheres have regained much interest in the last few years.[1-8] Modern methods of material analysis such as dynamic light scattering[9,10] or videomicroscopy[8,11,12] combined with techniques for sample preparation which were mainly influenced by polymer chemistry[13-15] provide scientists with almost ideal model systems, for example, monodisperse colloidal hard spheres. Suspensions of these materials in some ways show the same characteristics as atoms or molecules but on much larger time and distance scales, which means easier access to experimental results.[1]

[1] Institut für Physikalische Chemie, Johannes-Gutenberg-Universität Mainz, D-55099 Mainz, Germany.

0022-4715/94/0200-0687$07.00/0

Dynamical behavior of colloidal suspensions can be studied by various methods, for example, photon-correlation spectroscopy,[1,2,16,17] forced-Rayleigh scattering,[17] or digital image processing of images taken either from an ultramicroscope[8,11,12] or by fluorescence microscopy.[12] Nevertheless, since the samples which are currently available are only nearly monodisperse and the interactions between the colloidal particles and their influence on dynamics and structure are not yet fully understood, computer simulations also provide a useful tool to gain more detailed information concerning this matter.[18–21] One can also study idealized systems by numerical simulations which are not available experimentally, such as true two-dimensional samples,[12] to obtain information about the specific effect of certain parameters on structure and dynamics of the system of interest.

There are two different approaches to properties of atomic or molecular systems by computer simulations: the Monte Carlo method,[23] where physical quantities of the system are calculated from ensemble averages by calculation of many microstates of the system with the same particle number, volume, and energy, and the molecular dynamics (MD) technique,[23] which is based on the numerical solution of Newton's equations of motion. The MD calculations give a direct access to single-particle trajectories, which are our main interest. For simulations of colloidal suspensions additional terms have to be added which consider the interaction between the suspended particles and the surrounding molecules of the solvent. This leads to the so-called Brownian dynamics (BD)[24] calculations of colloidal systems, which are analogous to the MD simulations of molecular systems.

In this paper we are interested in colloidal hard-sphere suspensions. These systems have been the focus of many recent theoretical investigations and computer simulations.[18,25–31] The interaction pair potential of hard-sphere systems is not numerically integrable, so the Langevin equation for Brownian motion cannot be solved for such samples. Correspondingly, it is not possible to apply the standard BD algorithm[1,2,4] as used for Yukawa systems.[19–22] An alternative method for numerical treatment of hard-core interactions in colloidal suspensions was suggested by Cichocki and Hinsen,[18] who used a quasi Monte Carlo technique for Brownian motion in configuration space. In their algorithm, one sphere is chosen at random and displaced in the random direction by a distance which corresponds to N times the free Brownian motion during the nominal time step of the calculation cycle, N being the total number of particles in the sample. If particle overlap is found after this time step, the new configuration is ignored and the old one is stored, otherwise the new configuration is kept. The self-diffusion coefficients obtained by this procedure are systematically

too small for finite time steps. Reasonably accurate diffusion coefficients for sphere volume fractions up to $\varphi = 0.5$ were obtained by extrapolation from runs at different decreasing time steps. However, at high concentrations the mean nearest-neighbor spacings are so small that very small time steps, corresponding to very small steps of Brownian motion during one calculation period, are necessary to get suitable results. Thus, much computer time is required, and typically 5 hr on a CRAY XM-P 48 was needed for one φ value in the simulation of Cichocki and Hinsen.

In the present paper, we have developed a BD algorithm where the coupling of particle motion through finite-range interaction potentials is replaced by an appropriate procedure which accounts for hard-sphere collisions. Hydrodynamic interaction (see below) is neglected as was done in the simulation of Cichocki and Hinsen. During the time between collisions each particle moves by free Brownian motion independent of all other particles of the sample. We can therefore move every particle during one calculation cycle which defines one time step. Any particle overlap which occurs at the end of this time step is removed by a symmetric shift (Fig. 1) described in more detail in the following section. It turns out that the self-diffusion coefficients obtained by this procedure are systematically too large for finite time steps and higher concentrations. However, we can show that the convergence is by far superior to that of the previous Monte Carlo procedure[18] if judged by the computer time needed for achieving a particular accuracy. Comparable results are obtained with a PC and a MicroVAX, which both are more than 500 times slower than the CRAY used by Cichocki and Hinsen.[18] The main purpose of our work is to find efficient

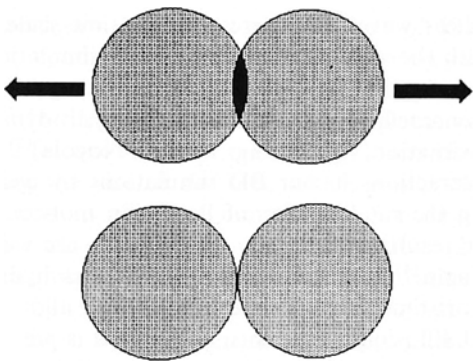

Fig. 1. Principle of the treatment of hard-core interactions during one calculation cycle of our BD algorithm. Accidental particle overlap is corrected by the symmetric shift of the interfering particles up to their touching distance.

ways to computer simulations of current experiments with hard-sphere colloids in concentrated solutions. We also present a practicable method for comparing the concentration dependence of diffusion in two and three dimensions. Hydrodynamic interactions are treated approximately in a manner proposed by Medina-Noyola.[5]

2. BASIC CONCEPTS

2.1. Interactions

In the usual colloid suspensions the mass of the diffusing particles is much larger than that of the surrounding liquid molecules. Correspondingly, the time scales relevant in standard BD simulations are much larger than the Brownian relaxation time $\tau_B = m/6\pi\eta_0 R$,[1] where R is the hydrodynamic radius, m the mass of the colloidal particle, and η_0 the solvent viscosity. For equal liquid and particle densities, $R = 0.5\ \mu$m, and $\eta_0 = 10^{-3}$ Pas, the parameters of our simulations yield $\tau_B = 5.5 \times 10^{-8}$ sec. Therefore, we can use the Einstein relation

$$\begin{aligned} \langle r(t)^2 \rangle &= 2dD_0 t \\ D_0 &= kT/6\pi\eta_0 R \end{aligned} \tag{1}$$

for calculating the mean square displacement for free Brownian motion. In Eq. (1), D_0 is the diffusion coefficient, d the dimensionality, and k the Boltzmann constant. At finite concentrations, diffusion is slowed down by hydrodynamic interactions between the moving colloid spheres and by hard collisions. Since hydrodynamic interactions propagate on the time scale of viscous shear waves, the corresponding time scale τ_H is very small in comparison with the smallest time step of BD simulations; at moderate concentrations $\tau_H \sim \tau_B$.[1] This justifies the assumption that only the short-time diffusion coefficient D_s is affected by hydrodynamic interactions in a first approximation. Following Medina-Noyola,[5] we incorporate hydrodynamic interactions in our BD simulations by using D_s instead of D_0 in determining the random step of Brownian motion or, alternatively, by factorizing the results with D_s/D_0. For D_s, we use values obtained by Beenaker and Mazur[4] in a treatment that includes hydrodynamic interactions in the short-time limit. This crude method allows for comparison with experimental diffusion coefficients, although it is probably not justified at very high concentrations. However, an explicit inclusion of hydrodynamic interactions in our calculations appears hopeless at the present state of the theory,[18,19] also considering the fact that our computer power is much too insufficient.

Since the interparticle potential is zero between the hard collisions our simulation is that for free Brownian motion of particles having the diffusion coefficient D_s except for the algorithm that accounts for the collisions.

2.2. Algorithm

In our simulations we start from some initial particle configuration, either purely random or a simple cubic lattice, and proceed as follows in each of the successive time steps τ:

1. Each particle is moved by the distance $(2D_s\tau)^{1/2}$ in one of the randomly chosen directions along the Cartesian axes ($\pm x$, $\pm y$, $\pm z$).
2. Any particle overlap detected after the move is corrected by pairwise shifting of the interfering particles up to their touching distances (see Fig. 1).

Although this shift may cause secondary overlaps with other particles in concentrated suspensions, this is ignored, and the next time step τ proceeds from the particle configuration obtained after the shifts. Since this procedure differs considerably from hard collisions in a real system, our algorithm cannot provide reasonable results unless the time step τ is chosen sufficiently small and the corresponding overlap distance very much smaller than the particle size. The errors introduced cancel in part on a coarse-grained time scale $\Delta t > 10^3\tau$; however, they become severe at very high concentrations. A detailed error analysis is given in the next section.

The following conditions were chosen in the numerical simulations: the sphere radius was chosen as $R = 0.5\ \mu$m, which corresponds to $D_0 = 4.4 \times 10^{-13}\ \text{m}^2\ \text{sec}^{-1}$ for free Brownian motion in water at 20°C. In the two-dimensional ($d = 2$) runs we chose a box of $32 \times 16 \times 1\ \mu\text{m}^3$ with periodic boundary conditions[23] in the x and y (not z) directions. The concentration was changed by varying the number of spheres from 48 to 528 in steps of 48.[12] In the $d = 3$ simulations we kept the particle number at $7^3 = 343$ ($8^3 = 512$ for one run with $\tau = 0.5$ msec), and changed the concentration by varying the size of the box, which was a cube with periodic boundary conditions in all three dimensions. For direct comparison of $d = 2$ and $d = 3$ particle dynamics we also performed $d = 2$ calculations with constant particle number 343, adjusting the concentrations (as in $d = 3$) by varying the size of the simulation area. As mentioned above, the initial particle configurations were chosen as a simple cubic lattice or some random distribution. The time steps τ for different runs were varied between 50 μsec and 10 msec, where the latter is still small in comparison with the "structural relaxation time"[1] $\tau_R = R^2/D_0 = 0.6$ sec. After an equilibration time of 5 sec all particle positions were stored as a function of

the diffusion time $t = n \times \tau$ at certain time intervals Δt, say, 0.1 sec. From these data the time-dependent self-diffusion coefficient $D(t)$ was determined from the mean square displacements

$$\langle [\mathbf{r}(t'+t) - \mathbf{r}(t')]^2 \rangle_{t',N} = 2dD(t)t \tag{2}$$

which corresponds to Eq. (1).

2.3. Error Analysis of the Algorithm

In this section we only discuss $d = 3$ results, since the convergence and also the characteristic errors of our algorithm do not depend on the dimensionality of the considered sample. We also had tested the role of our initial configuration and found that our results were not affected if the equilibration time was chosen large enough (> 2 sec). We also assured that our particle number was large enough by doing one run with more than 343 particles, say, 512, which did not change our results.

To give a detailed analysis of our algorithm we have determined the following quantities for runs with $N = 343$ at different particle concentrations and different time steps τ: the reduced short-time diffusion coefficient, $D(\tau)/D_0$, the number of pairwise particle overlaps before, $\mathrm{ov}(\tau\_)$, and after, $\mathrm{ov}(\tau)$, correction, the mean overlapping distance after correction, $d(\tau)$ [μm], and the number of overlapping particles before and after correction, $N(\tau\_)$ and $N(\tau)$. Every overlapping particle is counted only once. $N(\tau\_)$ is a measure of interparticle interactions, i.e., hard collisions, during our time step. We also calculated the long-time diffusion coefficient, $D(t = 5\ \mathrm{sec})/D_0$, in order to investigate the convergence of our algorithm with decreasing time step τ especially at higher concentrations. Some of our results are summarized in Tables I and II:

The short-time diffusion coefficients $D(\tau)/D_0$ shown in Table I represent the reduction caused by the overlap correction which pushes the overlapping particles partly back into the direction they had come from by free Brownian motion. Without corrections, $D(\tau\_)/D_0 = 1$, since hydrodynamic interaction is neglected. The reduction of $D(\tau)$ is partly canceled, since $D(t)$ is increased for $t > \tau$ by the effect of the secondary overlaps, $\mathrm{ov}(\tau)$, as discussed below. The efficiency of our hard collision algorithm can be estimated from the reduction of the number of overlaps from $\mathrm{ov}(\tau\_)$ to $\mathrm{ov}(\tau)$ [or that of the overlapping particles from $N(\tau\_)$ to $N(\tau)$] and the average overlapping distance $d(\tau)$ after the correction. Apparently, secondary overlaps play an important role at high concentrations and too large time steps τ.

In Table II we present some long-time results $D(t = 5\ \mathrm{sec})$ for various particle volume fractions and time steps τ decreasing from 10 to 0.1 msec.

Table I. Results for Characteristic Quantities Useful for a Detailed Discussion of the Errors of Our Algorithm

τ, msec	φ	$D(\tau)/D_0$	ov(τ_-)	ov(τ)	$N(\tau_-)$	$N(\tau)$	$d(\tau)$, μm	φ_{eff}
10	0.20	0.9510	51.7	32.4	92.4	56.9	0.0044	0.200
	0.30	0.9056	101.5	68.1	161.7	107.4	0.0080	0.298
	0.40	0.8409	180.6	133.8	239.0	180.5	0.0129	0.392
	0.50	0.7571	309.4	255.9	305.5	268.3	0.0187	0.479
1	0.20	0.9640	37.5	22.5	69.2	40.6	0.0026	0.200
	0.30	0.9286	74.6	47.3	126.2	79.0	0.0044	0.299
	0.40	0.8708	139.5	97.8	202.8	144.3	0.0073	0.397
	0.50	0.7853	249.1	192.8	280.4	230.9	0.0116	0.489
0.5	0.20	0.9724	27.3	15.5	51.4	29.0	0.0012	0.200
	0.30	0.9441	55.7	34.2	98.4	59.4	0.0026	0.300
	0.40	0.8985	104.5	67.0	164.4	105.3	0.0042	0.399
	0.50	0.8242	192.7	139.2	246.2	185.4	0.0067	0.495
0.1	0.20	0.9867	12.6	6.8	24.4	13.2	0.0002	0.200
	0.30	0.9730	26.3	15.0	49.6	28.0	0.0004	0.300
	0.40	0.9477	50.9	29.5	68.0	39.7	0.0007	0.400
	0.50	0.9009	98.7	61.4	156.5	98.3	0.0019	0.500

For comparison, the data of Cichocki and Hinsen[18] are also given. Whereas our results are in quite good agreement with ref. 18 up to volume fractions of 0.30 for all τ values (within a statistical error of $\pm 5\%$), we find much larger ($>15\%$) systematic deviations at higher concentrations ($\varphi \geqslant 0.40$). Our long-time diffusion coefficients are increasing dramatically with increasing τ. This can be understood from the presence of the secondary overlaps in the stored particle configurations, which means a reduction of the spacing of touching particles compared to the theoretical value $d = 2R$. Thus, the effective particle radius is smaller than 0.5 μm and, correspondingly, we have to consider effective volume fractions which,

Table II. Convergence of Long-Time Diffusion Coefficients $D(t = 5\,\text{sec})/D_0$ with Decreasing Time Step τ

τ, msec	$\varphi = 0.20$	$\varphi = 0.30$	$\varphi = 0.40$	$\varphi = 0.50$
10	0.660	0.532	0.406	0.244
1	0.674	0.532	0.361	0.184
0.5	0.678	0.499	0.340	0.164
0.1	0.684	0.503	0.334	0.128
ref. 18	0.64	0.48	0.29	0.09

depending on the number of overlapping spheres $N(\tau)$ and the distance $d(\tau)$ of the secondary overlaps, can be significantly decreased compared to the true values. It is obvious that these smaller effective volume fractions yield larger particle mobilities and larger long-time diffusion coefficients than expected theoretically. To discuss this fact in more detail, we give a simple formula for estimating these reduced effective volume fractions from the data given in Table I:

$$\varphi_{\text{eff}} = V_c^{-1}\{[N - N(\tau)]\, V_s + N(\tau)\, V_s[1 - d(\tau)/2R]^3\}$$
$$\approx \varphi[1 - 3N(\tau)\, d(\tau)/2NR] \tag{3}$$

V_s and V_c are the sphere and computing cell volumes, respectively. The results are given in the last column of Table I. Apparently, the effective particle volume fractions are decreased significantly at higher concentrations above 0.30 with increasing τ. This corresponds well to the other results given in Table I, and demonstrates that the secondary particle overlaps cause a systematic deviation of our long-time particle mobilities toward too large values. It should be noted that the diffusion coefficients of Cichocki and Hinsen given in Table II were obtained after extrapolation to zero step time.[18] We were not able to find a similar extrapolation formula for our data, since the negative and positive errors caused by the overlap correction affect $D(t)$ differently at different diffusion times t. A more detailed comparison of our results with those of Cichocki and Hinsen will be given below.

2.4. Comparison of Diffusion in Two and Three Dimensions

Although there are fundamental differences between diffusion in two and three dimensions (see next section), it is desirable to compare calculated diffusion coefficients at corresponding particle concentrations. Since our $d=2$ simulations are performed in a layer of thickness $2R$, we can define a $d=2$ volume fraction φ_2 which is related with the area fraction φ_A of circular disks in a plane by

$$\varphi_2 = 2\varphi_A/3 \tag{4}$$

It is apparent from Fig. 2 that the maximum volume fraction given by close packing of spheres in the layer is $\varphi_2^{(\max)} = \pi/(3\sqrt{3}) = 0.6046$, to be compared with $\varphi_3^{(\max)} = \pi/(3\sqrt{2}) = 0.7405$ for $d=3$ close packing. We have proposed[11] to compare $d=2$ and $d=3$ diffusion coefficients at volume fractions where the nearest-neighbor distances in the corresponding close-packing lattices are equal. This can be visualized in Fig. 2 by keeping the

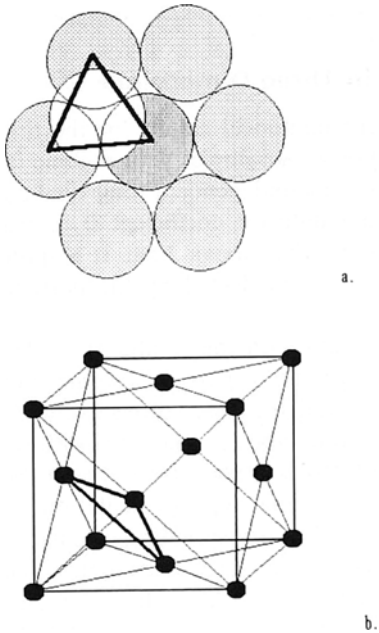

Fig. 2. Lattices for uniform distribution of spheres in $d=2$ and $d=3$ samples, based on the crystalline closed packed structures, respectively. The fat triangles in the $d=2$ trigonal lattice and the $d=3$ FCC lattice correspond, the length of one side equals the nearest-neighbor spacing.

sphere centers fixed at their lattice positions as the volume fraction is reduced by decreasing the sphere radii. The requirement of equal nearest-neighbor distance results in

$$\varphi_3 = 3^{5/4}(2\pi)^{-1/2}\,\varphi_2^{3/2} = 1.575\varphi_2^{3/2} \tag{5}$$

for rescaling φ_2 into a corresponding $d=3$ volume fraction φ_3. It should be noted that the $d=2$ layer in Fig. 2a corresponds to the (111) plane of the face-centered-cubic lattice in Fig. 2b, and the circle over the $d=2$ fat triangle becomes the origin of the $d=3$ lattice cell. The situation becomes more complex for spheres between two hard surfaces having a distance $d>2R$. In this case, there are several possibilities for close-sphere packings leading to hexagonal or quadratic phases of two or more layers. Computer simulations in such systems are planned which correspond to our current diffusion experiments in thin suspension layers.[11,12] It should be mentioned that Murray and co-workers[32] had used a similar procedure to compare their results obtained from digital image processing of thin layers of aqueous suspensions of charged spheres with 3D results.

3. RESULTS

3.1. Simulations in Three Dimensions

Figure 3 gives our numerical results for the time-dependent self-diffusion coefficient $D_s(t)$ of $d=3$ samples with volume fractions in the range of 0.10–0.60. The limit of time-independent long-time particle mobility characterized by the long-time diffusion coefficient D_L is reached for every sample at diffusion times t somewhat above 2 sec. It is quite remarkable that this limiting time seems to be unaffected by the particle concentration of the sample.

To compare our data with the results of ref. 18 in some detail, Fig. 4 presents our $d=3$ results for a particle volume fraction of $\varphi=0.40$ from runs with $\tau=1.0$, 0.5, and 0.1 msec, respectively. Also shown are results from ref. 18 at the same volume fraction with calculation parameters $\lambda=0.035$, 0.025, and 0.018, respectively (from below), representing a numerical measure of the time step of calculation τ. From Eqs. (14)–(17), (20), and (21) of ref. 18 the corresponding calculation time steps τ for our simulation parameters (D_0, R, N) can be determined easily, giving 0.37, 0.19, and 0.1 μsec, respectively. Also shown is the curve Cichocki and Hinsen had obtained by extrapolation of their data to $\lambda=0$ (corresponding to $\tau=0$). As mentioned above, finite τ values lead to too large $D(t)/D_0$ in our case due to secondary particle overlaps, whereas Cichocki and Hinsen obtain too small values for finite λ. It is apparent from the comparison that our procedure converges at τ values more than 1000 times larger than that of Cichoki and Hinsen, although we have a structural error due to secondary overlap which is avoided in ref. 18, where only one particle is

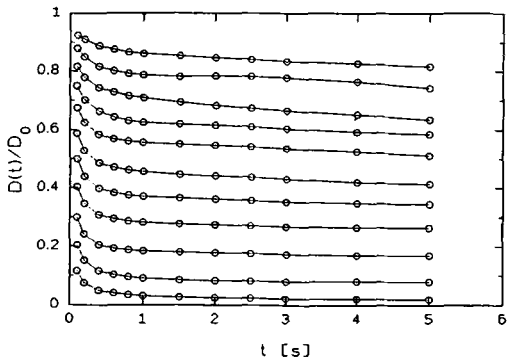

Fig. 3. Time-dependent reduced self-diffusion coefficients, determined for $d=3$ samples with volume fractions $\varphi=0.10$–0.60 (in steps of 0.05, from above), with calculation period $\tau=0.5$ msec (open symbols; the lines are guides to the eye).

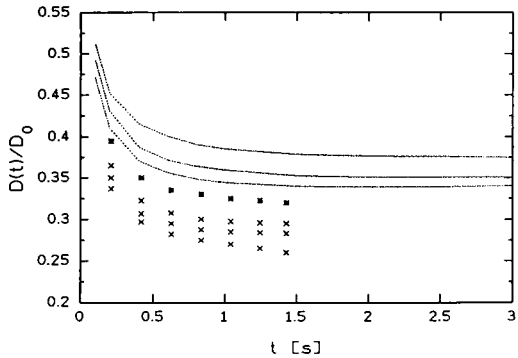

Fig. 4. Time-dependent reduced self-diffusion coefficient, determined with calculation periods $\tau = 1.0$, 0.5, and 0.1 msec (from above), for $d = 3$ samples with $\varphi = 0.40$ (dotted lines). For comparison results from ref. 18 are also presented for different values of the calculation parameter λ (see text) (crosses) and for the extrapolation $\lambda \approx 0$ (asterisks).

moved at a time and any move leading to overlap is omitted. This means our algorithm is much more efficient on the basis of comparable computer time. This was the main reason we could do our calculations on 68030-processor computers, even at very high particle concentrations up to closest packing.

In Fig. 5 we present our numerical results for the long-time diffusion coefficient D_L (asterisks) as a function of the $d = 3$ volume fraction [corrected for secondary particle overlaps; cf. Eq. (3)], including hydro-

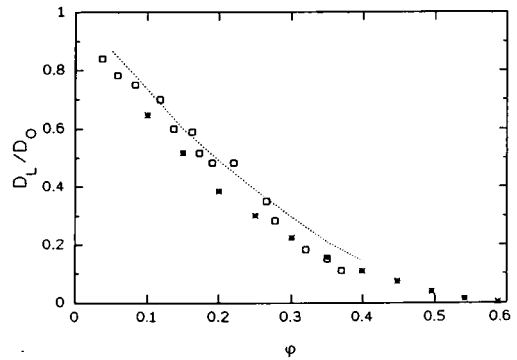

Fig. 5. Long-time self-diffusion coefficients from our BD simulations at various concentrations, including hydrodynamics following ref. 5, with volume fractions corrected for secondary overlaps (asterisks), compared with theoretical predictions (dotted line[5]) and light scattering experiments (open squares[33]).

dynamic interactions by factorization of our numerical data with the short-time diffusion coefficients from ref. 4 due to the suggestion of Medina-Noyola,[5] in comparison with experimental results obtained by dynamic light scattering[33] (squares). Also given are theoretical predictions for the concentration dependence of the reduced longtime self-diffusion coefficient D_L/D_0 by Medina-Noyola.[6] Although, there are small systematic differences, the agreement is remarkably good in view of the crude assumptions made in the simulations.

Figure 6 shows a comparison of our numerical D_L values (corrected volume fractions, see above), including hydrodynamic interactions (see above), with diffusion coefficients which were experimentally obtained by forced Rayleigh scattering on samples of dye-labeled spherical polystyrene microgels[15,17] of diameter ~ 200 nm, in the solvent bitolyl. The measurements were done in our group by S. Möller at samples up to very high concentrations. Included is a Mooney fit,[17] $\log D_L = A/(1 - B\varphi^{-1})$, of the experimental results. As in Fig. 5, our numerical data show very good agreement with experiment even at higher concentrations, but one should be aware of the logarithmic scale of the given results and the scattering of the experimental data. It should also be noted that the polydispersity and the network structure of the spherical microgels may result in increased diffusion coefficients in comparison with monodisperse hard spheres at high concentrations. This increase may accidentally be of the same order as the errors of our simulation, which also increase with increasing concentration.

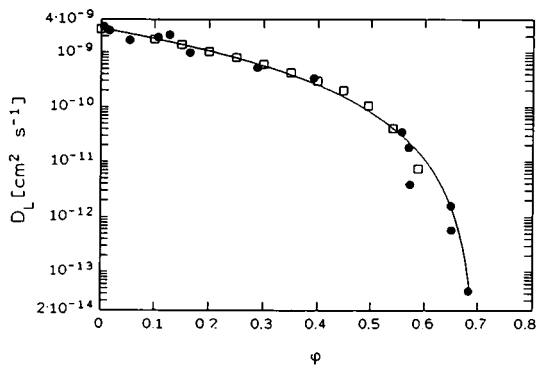

Fig. 6. Comparison of long-time self-diffusion coefficients at various volume fractions from $d = 3$ BD simulations (open squares) with experimental data from ref. 17 (full circles). Numerical results were factorized with D_s/D_0 to take into account hydrodynamic interactions following ref. 5; volume fractions were corrected for secondary particle overlaps. Also included is the Mooney fitting curve from ref. 17 (line).

After we have shown the validity of our numerical $d=3$ results by detailed comparison with experiments[17,33] and simulations,[18,34] we present our studies concerning the dimensionality and concentration dependence of particle mobilities by numerical simulations of $d=2$ and $d=3$ samples at corresponding volume fractions in the following section.

3.2. Comparison of $d=2$ and $d=3$ Samples

Figure 7 shows our results for $N(\tau_-)$, the number of particles with hard-sphere interactions during one cycle of calculation, for $d=3$ and $d=2$ samples with various τ ranging from 0.1 to 10 msec (see also the discussion of Table I given above). All particle concentrations have been corrected for secondary particle overlaps [cf. Eq. (3)] and the $d=2$ results are plotted versus the area fractions φ_A, whereas the $d=3$ values are plotted versus volume fractions. It should be mentioned that we tried to determine the interaction frequency, defined as extrapolation of the product of the number of particle overlaps, $\mathrm{ov}(\tau_-)$, and the number of cycles per second, τ^{-1}, as a quantity for τ-independent characterization of the intensity of particle interactions. Since we found no convergence down to $\tau=0.1$ msec and we were not able to choose smaller τ due to lack of computer power, we

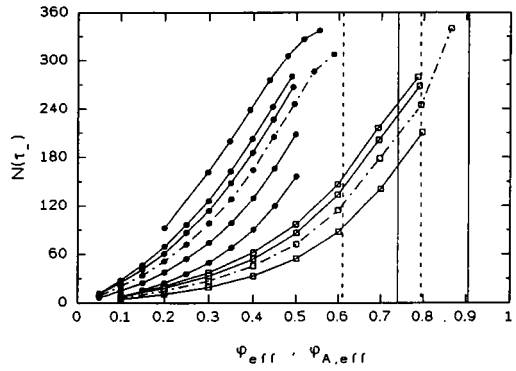

Fig. 7. Number of particles with interactions during one calculation step, $N(\tau_-)$, for simulation runs of $d=2$ and $d=3$ samples with various particle concentrations and calculation steps τ. All concentrations have been corrected for secondary overlaps [Eq. (3)]. The $d=3$ results (lines with full circles) are plotted versus their volume fractions, τ ranging from 0.1 to 10 msec (from below). The $d=2$ results (lines with open squares) are plotted versus the area fractions with τ ranging from 0.25 to 1 msec (from below). Symbols with dashed lines both correspond to $\tau=0.5$ msec. Vertical dashed lines mark volume fraction of $d=3$ random closed packing, $\varphi\approx 0.61$, and the corresponding [Eqs. (4), (5)] area fraction; vertical full lines correspond to the particle fractions of crystalline closed packings.

decided to present $N(\tau_-)$ as characteristic quantity. One can easily imagine that $N(\tau_-)$ strongly increases with increasing τ, in correspondence with the increasing distance the particles are moving by free Brownian motion. Although the strong dependence of our data on τ is seen in Fig. 7, all $d=3$, and, respectively, $d=2$ values show a tendency toward 100% interacting particles $[N(\tau_-)=343]$ at the same particle concentrations, $\varphi_3 \approx 0.61$ for $d=3$ and $\varphi_A \approx 0.88$ for $d=2$. These volume fractions should resemble closest packed structures, since no particle can be found moving without any collision with its nearest neighbors, not even for the smallest values of τ. For semiquantitative analysis, four perpendicular lines are drawn in Fig. 7, the full lines representing the crystalline closest packings with FCC ($d=3$) and trigonal ($d=2$) structure. The dashed line at $\varphi \approx 0.61$ signifies the random closed packing predicted by many authors for $d=3$ samples and identified with a glass transition.[1,35] The line at $\varphi \approx 0.795$ marks the corresponding $d=2$ area fraction, determined following Eqs. (5) and (4), where, however, no glass transition is indicated by the $N(\tau)$ values. To summarize the results of Fig. 7, we find different behavior considering the intensity of interparticle interactions in $d=3$ and $d=2$ samples. Whereas in $d=3$ a closed packed structure with 100% interacting particles is reached at a volume fraction far below the closest crystalline FCC packing which could be described as a glass transition with random closed packing structure, in $d=2$ the intensity of interactions is comparably small up to

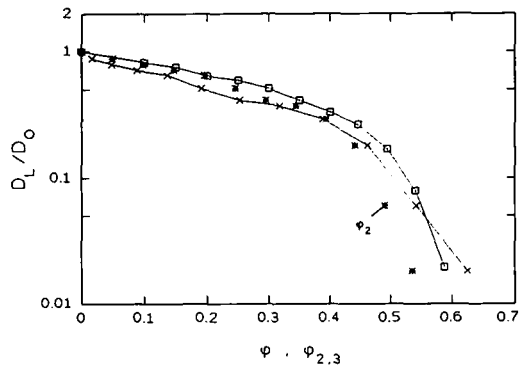

Fig. 8. Concentration dependence of long-time self-diffusion coefficients for two- (crosses, asterisks) and three-dimensional samples (open squares). The $d=2$ results are plotted versus original $d=2$ volume fractions φ_2 (asterisks) and versus their corresponding $d=3$ particle concentrations φ_3 (crosses), which were calculated from Eq. (5) after the principle discussed at length in the text. Dotted lines are a guide to the eye to visualize the crossover (see text) at $\varphi \sim 0.55$. All volume fractions have been corrected for secondary particle overlaps [Eq. (3)].

volume fractions close to the trigonal crystalline structure, and no glass transition can be found, opposite to the $d=3$ results.

In Fig. 8 we show the concentration dependence of the long-time diffusion coefficient, $D_L(\varphi)$, for $d=2$ and $d=3$ samples. The $d=2$ results are plotted versus the original $d=2$ volume fractions φ_2 and versus the corresponding rescaled $d=3$ values φ_3 [see above, Eqs. (4), (5)]. It should be noted that all particle concentrations have been corrected for secondary overlaps as above in Figs. 5 and 6. Comparison of the rescaled $d=2$ data and the $d=3$ results concerning the influence of sample dimensionality on particle mobility shows smaller diffusion coefficients of the $d=2$ samples at small concentrations, whereas the opposite is found at very high concentrations above $\varphi_3 \sim 0.55$. These findings could be interpreted as following:

1. Consider diffusion in the xy plane. In $d=2$ the third degree of freedom of motion is missing, which leads to more effective caging of the moving particles due to hard-sphere interactions with their six in-plane neighbors. Thus we find less particle mobility in $d=2$ samples compared with $d=3$, where the in-plane cage can relax also by particle motion in the z direction.
2. At very high concentrations, $\varphi_3 > 0.55$, we find larger particle mobilities in $d=2$ than in $d=3$ due to the difference in phase behavior of $d=2$ and $d=3$ samples as mentioned above. At $\varphi \approx 0.61$ a $d=3$ glass transition exists where all long-time particle mobility ceases. In $d=2$ no similar random closed packing is found,[36] which means some particle mobility should remain until the volume fraction of the closed packed crystalline structure is reached at $\varphi_3 \sim 0.741$.

4. CONCLUSIONS

We have presented a new very effective algorithm for BD simulation of colloidal hard-sphere systems. The long-time self-diffusion coefficients we have determined by numerical simulation of the single-particle trajectories of $d=3$ samples agree well with numerical results of Cichocki and Hinsen[18,34] at not too large volume fractions. Our data also agree with various experimental results. Comparing simulations of two- and three-dimensional samples at corresponding particle volume fractions, we find differences in the intensity of particle interactions, $N(\tau_-)$, and the concentration-dependent long-time self-diffusion coefficients. At small concentrations the caging of nearest neighbors seems to be more effective in $d=2$ than in $d=3$, which leads to a smaller particle mobility in $d=2$, whereas at very large volume fractions, $\varphi > 0.55$, close to the $d=3$ glass transition

a crossover is found and the mobility in $d=3$ decreases dramatically. The fact that particles in $d=2$ show a higher mobility (compared to $d=3$) at very large volume fractions φ_3 above the $d=3$ glass transition seems to indicate that no glass transition is found in $d=2$ hard-sphere systems, which corresponds to the results given in ref. 36. Nevertheless, there might be other possibilities of interpretation, as, for example, the theoretical lack of any freezing effects in $d=2$ beyond $\varphi_3=0.741$, whereas such freezing effects, which lead to a dramatic decrease of the particle mobility, are generally predicted in $d=3$ samples at volume fractions beyond the glass transition.[1] For clarification, the equilibrium structures of our BD simulation results have to be investigated, which will be a matter for a future publication.

The results we have given are only averaged single-particle mobilities or self-diffusion coefficients. The main reason for this is that our accompanying studies of digital image particle tracking were restricted to diffusion of labeled tracer particles at higher concentrations.[11] However, recent advances in preparation of optical core shell systems[37,38] will allow experimental studies where the core volume fraction is only a few percent whereas the shell provides for high concentrations up to random or crystalline close packings. The situation is then similar to that in charged colloid systems where the "shell" is given by electrostatic repulsion.[39] Thus, the dynamic structure can be investigated in real space by light microscopy if the shell is made invisible by index matching with the solvent and has a thickness ($\gtrsim 300$ nm) that allows for optical resolution of the distance of neighboring cores in concentrated suspensions. The efficient algorithm presented in this paper should allow for most computer simulations desirable for analyzing these experiments by using a work station which is about 100 times faster than a good PC.

ACKNOWLEDGMENT

Financial support by the Stipendienfonds der Chemischen Industrie is gratefully acknowledged.

REFERENCES

1. P. N. Pusey, in *Liquids, Freezing and the Glass Transition*, D. Levesque, J. P. Hansen, and J. Zinn-Justin, eds. (Elsevier, Amsterdam, 1991).
2. W. van Megen, R. H. Ottewill, S. M. Owens, and P. N. Pusey, *J. Chem. Phys.* **91**:552 (1989).
3. A. van Veluwen, H. N. W. Lekkerkerker, C. G. de Kruif, and A. Frij, *J. Chem. Phys.* **89**:2810 (1988).

4. C. W. J. Beenakker and P. Mazur, *Physica* **126A**:349 (1984).
5. M. Medina-Noyola, *Phys. Rev. Lett.* **60**:2705 (1988).
6. H. Yoshida, K. Ito, and N. Ise, *J. Am. Chem. Soc.* **112**:592 (1990).
7. J. T. G. Overbeek, *J. Chem. Phys.* **87**:4406 (1987).
8. C. A. Murray, D. H. van Winkle, and R. A. Wenk, *J. Phys. Cond. Matter* **2**:SA385 (1990).
9. B. J. Berne and R. Pecora, *Dynamic Light Scattering* (Wiley, New York, 1976).
10. R. Pecora, *Dynamic Light Scattering* (Plenum Press, New York, 1985).
11. W. Schaertl, Ph.D. thesis, Mainz (1992).
12. W. Schaertl and H. Sillescu, *J. Colloid Interface Sci.* **155**:313 (1993).
13. E. B. Bradford and J. W. Vanderhoff, *J. Appl. Phys.* **26**:864 (1955).
14. J. W. Vanderhoff, *Prepr. Am. Chem. Soc. Div. Org. Coat. Plast.* **24**:223 (1964).
15. M. Antonietti, W. Bremser, D. Müschenborn, Ch. Rosenauer, B. Schupp, and M. Schmidt, *Macromolecules* **24**:6636 (1991).
16. E. Bartsch, M. Antonietti, W. Schupp, and H. Sillescu, *J. Chem. Phys.* **97**:3950 (1992).
17. E. Bartsch, S. Möller, F. Renth, and H. Sillescu, *Physica A*, in press.
18. B. Cichocki and K. Hinsen, *Physica A* **166**:473 (1990).
19. H. Löwen, J. P. Hansen, and J. N. Roux, *Phys. Rev. A* **44**:1169 (1991).
20. N. Pistoor and K. Kremer, *Prog. Colloid Polym. Sci.* **81**:184 (1990).
21. M. O. Robbins, K. Kremer, and G. S. Grest, *J. Chem. Phys.* **88**:3286 (1988).
22. N. Pistoor, Ph.D. thesis, Mainz (1992).
23. H. Gould and J. Tobochnik, *An Introduction to Computer Simulation Methods, Part 1* (Addison-Wesley, Reading, Massachusetts, 1988).
24. D. L. Ermak and J. A. McCammon, *J. Chem. Phys.* **69**:1352 (1978).
25. E. G. D. Cohen and I. M. de Schepper, *J. Stat. Phys.* **63**:241 (1991).
26. H. Löwen and G. Szamel, *J. Phys. Cond. Mat.* **5**:2295 (1993).
27. B. J. Ackerson and L. Fleishman, *J. Chem. Phys.* **76**:2675 (1982).
28. H. N. W. Lekkerkerker and J. K. G. Dhont, *J. Chem. Phys.* **80**:5790 (1984).
29. J. A. Leegwater and G. Szamel, *Phys. Rev. A* **46**:4999 (1992).
30. G. Szamel and J. A. Leegwater, *Phys. Rev. A* **46**:5012 (1992).
31. B. Cichocki, *Physica A* **148**:165 (1988).
32. C. A. Murray, W. O. Sprenger, and R. A. Wenk, *Phys. Rev.* **42B**:1169 (1991).
33. W. van Megen and S. M. Underwood, *J. Chem. Phys.* **91**:552 (1989).
34. B. Cichocki and K. Hinsen, *Physica A* **187**:133 (1992).
35. L. V. Woodcock, *Ann. N. Y. Acad. Sci.* **37**:274 (1981).
36. B. D. Lubachevsky, F. H. Stillinger, and E. N. Pinson, *J. Stat. Phys.* **64**:501 (1991).
37. A. van Blaaderen and A. Vrij, *Langmuir* **8**:2921 (1992).
38. V. Frenz, A. Kasper, W. Schaertl, and H. Sillescu, work in progress.
39. C. A. Murray, W. O. Sprenger, and R. A. Wenk, *Phys. Rev. B* **42**:1169 (1991).